CHAPTER 2

MICRO-MECHANICAL MODEL

Relations between microstructure and property are at the heart of modern material engineering. They are beneficial to material improvement. A favorable performance can be obtained by adjusting characteristics of its components. However, due to the highly complex structure of concrete, such relations have been not so clearly illustrated.

Concrete is heterogenous material, comprising aggregate particles randomly embedded in cementitious matrix. Even in each phase, properties of concrete vary from one position to another in the entire domain. It is very difficult to analyze concrete behavior in a continuous manner. Progressive cracking mechanism and non-linear characteristics also make the concrete response more sophisticated. With different failure criteria and numerical approaches, many simulation models have been developed to describe such behaviors.

In this chapter, a simply, but reasonable model of concrete microstructure will be developed in order to simulate the response of concrete subjected to static monotonic loading, especially in compression. Fracture mechanics and finite element analysis will be used as a potential tool. Afterwards, a parametric study of concrete component features will be performed to evaluate feasibility to produce concrete with compressive strength greater than 150 MPa. If possible, the required properties of concrete components will be finally indicated.

2.1 Failure Mechanism of Concrete

Failure responses of concrete material subjected to different loading conditions are governed by the initiation and propagation of internal cracks during loading. When a concrete specimen is initially loaded, distributed microcracks are randomly formed throughout the specimen. These microcracks begin to increase in length, width, and numbers beyond the proportional limit, causing deviation of stress to strain ratio. After that, the microcracks begin to

localize into a macrocrack that critically propagates at the peak stress. Strain softening is observed under the propagation of this crack.

To model this behavior using discrete crack fracture mechanics, it is assumed that an initial crack begins to propagate when the stress at that point is exceeding its tensile strength (f_t). When the crack extends in concrete, new crack surfaces are formed along the path of the initial crack tip. The newly formed crack surfaces may be in contact and are tortuous in nature, leading to toughening mechanisms in the fracture process zone. They may continue to sustain some normal tensile stress, which is characterized by stress-separation relationship (Jenq and Shah, 1985), as shown in Fig. 2.1. Thus, mathematically, the energy release rate required to propagate crack (G_q) is the summation of the energy rate consumed in creating cracking surfaces (G_{Ic}) and the energy rate to overcome cohesive pressure in separating the surfaces (G_σ), i.e.,

$$G_q = G_{Ic} + G_\sigma \tag{2.1}$$

The value of G_{Ic} may be evaluated based on linear elastic fracture mechanics (LEFM) and is called critical energy release rate. Since G_σ is equal to the work done by the cohesive pressure over a unit length of the crack with a unit thickness, its value can be calculated as

$$G_\sigma = \int_0^{w_t} \sigma(w)dw \tag{2.2}$$

where w_t is the displacement at the initial crack tip.

With the concept of the fictitious crack model (Hillerborg et al, 1976), it is assumed that the energy needed to create the new surfaces is small compared to that required to separate them, the energy rate term G_{Ic} vanishes. Furthermore, the upper integral limit w_t should be replaced by critical crack separation displacement (w_c) for $w_t > w_c$. Then, eq. (2.1) becomes

$$G_q = \int_0^{w_c} \sigma(w)dw = G_F \tag{2.3}$$

The integral in eq. (2.3) is the area under stress-separation curve, and is denoted as G_F . The material fracture toughness G_F represents the energy absorbed per unit area of crack and is regarded as a material fracture parameter. It is noted that when the shape of $\sigma(w)$ is given, the material fracture property can be determined by the values of f_t and G_F . In this study, linear decay of stress-separation curve is assumed, resulting in

$$w_c = \frac{2G_F}{f_t} \tag{2.4}$$

The finite element method is a powerful tool to analyze such cracking behavior of the entire concrete specimen from a microstructural viewpoint. It is necessary to link the stress-separation relation to the constitutive equation. Based on the smeared crack model (Bazant and Oh, 1983), the ultimate strain (ε_u) is easily computed by introducing the element size (h_c), i.e.,

$$\varepsilon_u = \frac{w_c}{h_c} \tag{2.5}$$

The element size is helpful to make the model independent on mesh number and specimen scale (Bazant and Planas, 1998). The approach to determine this element size will be discussed in the following section.

2.2 Simulation of Concrete Behavior

Based on the ideas presented in the previous section, simulations of concrete response for this study will follow the algorithm that shown in the flowchart of Fig. 2.2. Details in each step will be described as following:

1.) Define aggregate arrangement

For the sake of simplicity, only circular aggregate is considered in this study. According to a given size distribution, aggregate particles are randomly generated in a two-dimensional concrete domain by a procedure previously used by Bazant et al (1990). The largest particles are placed first by assuming a uniform probability distribution, following by the next smaller size. The clearance of 1 mm between aggregate particles and of 0.5 mm between particles and specimen boundaries are reserved to prevent overlapping and stress singularity. The sample of the modeled internal structure is shown in Fig. 2.3.

2.) Discretize the entire specimen

The quadratic triangular element with straight sides and midside nodes is implemented to represent the whole domain of concrete in two dimensions. The finite element mesh is generated based on Delauney triangulation (de Schutter and Taerwe, 1993). To force the mesh to coincide with aggregate and specimen boundaries, a number of points and line segments are introduced before mesh generation. The distances between the prescribed points on aggregate boundaries play a dominant role in determining fineness of the mesh. An example of mesh generation is shown in Fig. 2.4. Elements in the ring area represent interface zone around aggregate particles.

3.) Assign material properties and constitutive relations

Four material properties for each phase are involving in the simulation, i.e., tensile strength (f_t), elastic modulus (E), Poisson's ratio (μ), and fracture toughness (G_{fc}). Because the failure pattern of concrete specimens is a result of the combinations of tensile cracking at micro level, it is assumed that stress-strain relation of elements under compressive and shear stress is perfectly linear elastic. While, that under tensile stress is linear up to tensile strength (f_t) and follows by linear-decay softening afterwards. The ultimate strain (ε_u) is calculated from eq. (2.5). The element constitutive relations are depicted in Fig. 2.5.

It is also realized that upon the localization of deformation, parts of the concrete specimen outside the localized zone unload. The plastic model will be applied here. In such a model, the unloading slope follows the same initial elastic modulus. It means that degradation in material properties is related only by the residual plastic strain.

4.) Calibrate the model

Since the concept of crack band (Bazant and Oh, 1983) is applied in the model, it is necessary to calibrate the model to evaluate the element size (h_c). This is accomplished by assuming the element size as a function of element area. The calibration is performed based on axial elastic modulus testing. This step involves assigning the same elastic modulus to all elements and applying a prescribed infinitesimal uniform deformation at one end, while the other end is held fixed in the loading direction and free in the perpendicular direction. The boundary conditions are illustrated in Fig. 2.6. By calculating the reaction at the fixed end, the resulting elastic modulus of the specimen can be evaluated.

5.) Perform simulation and analyze the output

As a commercial finite element analysis program with striking integrity, ANSYS® 5.4 will be used as a tool for the computer simulation. ANSYS® 5.4 is advantageous in performing non-linear analysis with user-defined material elements. Moreover, It is well familiar to crack simulation. There is also much flexibility in adjusting involving parameters and decisive algorithms. However, a difficulty in pre- and post-processor may impede such a simulation.

With ANSYS® 5.4 , the simulation will be performed with displacement control. That is, deformation will step-by-step grow at one end, while the other end is held fixed in the loading direction and free in the perpendicular direction. The simulation will be terminated when the

element strain is out of limit, making the iteration diverged. For each load step, the internal stress of all elements will be saved, and thus reactions as well as applied stress can be determined. Afterwards, the overall stress-strain relation of the concrete specimen under loading is obtained.

2.3 Compressive Response of Concrete

The compressive behavior of 100x100-mm concrete specimen will be simulated. At first, the same aggregate configuration as shown in Fig. 2.3 is concerned. The ratio of amount of aggregate with 10 mm diameter to that with 20 mm diameter is 60:40, so that aggregate contains approximately 64% of the whole specimen area. The finite element mesh is shown in Fig. 2.7.The material properties of each phase are given in Table 2.1. In this first simulation, the interface is neglected by assigning the properties of the bulk matrix.

The simulated stress-strain response is depicted in Fig. 2.8. It can be observed that the concrete specimen behaves almost linearly up to 60 percent of the ultimate load, and then followed by a non-linear part. The degree of non-linearity increases with increasing displacement until the ultimate load is attained. Thereafter, the specimen softens and the load-carrying capacity gradually deteriorates until the specimen fails. The failure pattern of the specimen is shown in Fig. 2.9. Though the model considered only tensile failure at the micro level, the shear band type of cracking can be noticed, reflecting reasonable failure mechanism in modeling. It is also seen that cracks mostly propagate at the interface around aggregate particles. Even with no difference between interface and matrix, the interface still play a significant role in controlling concrete behavior.

The dependency of the results on mesh size or number of elements, or the so-called mesh sensitivity, is a serious problem normally found in finite element models. To check this, three different meshes are generated with the same aggregate arrangement and material properties. The numbers of elements are 10012, 20136 and 40148 elements. The ratio is more or less 1:2:4. The simulated stress-strain relations of all three models are shown in Fig. 2.10. There is a convergence of stress value for a given strain when the number of elements increases. This mesh sensitivity is owing to the existence of element size in the model (Bazant and Planas, 1998).

With a given size distribution, aggregate particles are normally located randomly in the specimen domain. To investigate this uncertainty, four different patterns of aggregate

arrangement are prepared for the simulation, as shown in Fig. 2.11. Size distribution and fraction area of aggregate in concrete are reserved. The last pattern of aggregate arrangement represents the case of aggregate segregation. Fig. 2.12 shows the simulated stress-strain curves of these four models. The predicted response follows the similar trend. The difference in the ultimate loads of the aggregate pattern no. 1 to no. 3 is within 5%, whereas the ultimate loads of the aggregate pattern no. 4 is about 10% lower than the average of the others.

Variation in compressive response of concrete specimens with different size, which is shown in Fig. 2.13, is plotted in Fig. 2.14. The specimen dimensions are 50x50 mm, 100x100 mm, and 150x150 mm. It is obvious that the predicted stress value reduces when specimen size increases. This agrees with the Weibull theory on the weakest link (Mihashi and Izumi, 1977).

2.4 Verification with Experimental Results

The experiment is done to check for the accuracy of the proposed model. Three mixes of mortar are consisted of ordinary Portland cement, silica fume, river sand with fineness modulus of 3.04, tap water, and napthalene-based superplasticizer. The water/cement ratio is varied for each mix in order to produce mortars with significantly different strength. They are 0.30, 0.25, and 0.20. For all mixes, silica fume is added by 15% by weight of cement to improve the performance of the interface zone, while sand/cement ratio is about 1.0. Superplasticizer is applied to guarantee the flow value of 150%.

To produce concrete, these mortars will be blended with limestone coarse aggregate. The maximum aggregate size is about 20 mm, and the fraction of coarse aggregate smaller than 10 mm in diameter are approximately 60%. The mix proportion of mortars and concrete is tabulated in Table 2.2.

Tensile strength, elastic modulus, Poisson's ratio and fracture toughness of mortars and coarse aggregate are evaluated. In the case of mortars, they are tested at the age of 28 days. Direct tensile strength of briquette specimens is performed according to ASTM C190. Compression of 50x50x50-mm specimens is used for evaluating elastic modulus and Poisson's ratio. The longitudinal and transverse strain are detected by strain gauges. While, conforming to the suggested method of RILEM (1985), 40x40x160 notched prisms are performed in a three-point bend test to figure out the fracture toughness. The mortar test results are shown in Table 2.3. The

average 28-day tensile strength is 5.2, 7.8 and 9.2 MPa for water/cement ratio of 0.30, 0.25 and 0.20, respectively. Slight differences in Poisson's ratio and fracture toughness can be detected.

Rock cylindrical specimens with a diameter of 100 mm are cored from the aggregate quarry to test for their splitting tensile strength, elastic modulus, and Poisson's ratio. The test for splitting tensile strength follows ASTM C496, whereas ASTM C469 is applied for measuring elastic modulus and Poisson's ratio. The fracture toughness is determined by bending a sawed rock beam with a notch at midspan, according to ISRM (1988). The test results are also shown in Table 2.3. The splitting tensile strength is 20.8 MPa, elastic modulus is 98.2 GPa, Poisson's ratio is 0.17 and fracture toughness is 0.09 N/mm.

The concrete behavior is examined also at the age of 28 days. According to ASTM C469, 150x150x150-mm specimen is employed for compressive test by the displacement-controlled universal testing machine. The axial deformation is detected both by mechanical dial gauges and electrical strain gauges. The stress-strain curves for all three concrete mixes are depicted in Fig. 2.15. For the entire response, there is a good agreement in both stiffness and strength between the experimental result and the simulated one. As seen in Fig. 2.16, the similar failure pattern as in simulation, i.e. shear band cracking, is suspected.

2.5 Effect of Concrete Components' Properties

The understanding in influence of the component properties on the overall concrete characteristics provides valuable information on how to engineer concrete-making materials towards improved performance. In this section, the input parameters used in concrete modeling will be varied without interference of different aggregate configuration and finite element mesh. The finite element model that is shown in Fig. 2.7 is applied throughout the simulations in this parametric study.

2.5.1 Effect of Aggregate Properties

Firstly, to evaluate the effect of aggregate elastic modulus, the modulus has been changed dramatically to cover both practical and extreme margins. Shown in Fig. 2.17 are the simulated responses of varying aggregate elastic modulus from 10 to 120 GPa, corresponding to the modulus ratio of aggregate to matrix equal to 1/4-3. An increase in the elastic modulus of aggregate obviously raises the modulus of concrete, but reduces the degree of non-linearity. The

compressive strength of concrete seems maximum when the aggregate modulus equals to the matrix one. A drastic drop is found when the ratio of aggregate to matrix elastic modulus is less than 1.0.

The effect of aggregate tensile strength differing from 8 to 40 MPa is illustrated in Fig. 2.18, in which the aggregate tensile strength is up to 5 times of the matrix. The same concrete elastic moduli are observed, but the deviations from linearity occur at different strength levels. Increasing the tensile strength of aggregate increases concrete compressive strength within a certain limit. An approximately the same ultimate strains of concrete specimens are also detected.

It is shown in Fig. 2.19 that the difference in fracture toughness in the range of 0.04 and 0.12 N/mm does not change considerably the peak stress of concrete, but alters the post-peak behavior as well as the ultimate strain. For Poisson's ratio ranging from 0.1 to 0.3, no significant discrepancy in the simulated stress-strain curve of concrete is reported in Fig. 2.20.

2.5.2 Effect of Matrix Properties

By varying the matrix elastic modulus between 10 and 160 GPa, about 1/8 to 2 times of aggregate modulus, in Fig. 2.21, the improvement in elastic modulus of concrete is found corresponding to the increase in the matrix modulus. The highest compressive strength takes place when the ratio of aggregate to matrix modulus equals to 1. Fig. 2.22 shows the compressive response of concrete with matrix tensile strength of in between 2 and 16 MPa. Like aggregate tensile strength, compressive strength of concrete enhances when the tensile strength of matrix enlarges.

It is shown in Fig. 2.23 that ductility of concrete seems to improve when tensile fracture toughness increases. But, there is no effect on the overall elastic modulus and compressive strength. The ffect of varying Poisson's ratio of matrix is also negligible, as seen in Fig. 2.24.

2.5.3 Interaction on Concrete Strength

It is already demonstrated that enhancement in concrete compressive strength is dominated by improvement in the tensile strength of both aggregate and matrix. An increase only in tensile strength of each phase has a limited effect on the overall concrete strength. The chart in Fig. 2.25 is a interaction between tensile strength of aggregate and matrix on concrete strength obtained from the proposed simulation model. This interaction reveals the possibility to

manufacture concrete with each strength level. For example, ulra-high strength concrete with compressive strength higher than 150 MPa requires aggregate with tensile strength at least 16 MPa and matrix with tensile strength higher than 8 MPa. These tensile strength values may be a guideline in qualifying the potential materials for making ultra-high strength concrete. Therefore, to achieve ultra-high strength, the development of matrix and selection of coarse aggregate with tensile strength greater than such values will be discussed in the following chapters.

Table 2.1 Material properties for simulating compressive response

Phase	E (GPa)	f_t (MPa)	G_F (N/mm)	ν
Aggregate	80	16	0.080	0.15
Matrix	40	8	0.064	0.25
Interface	40	8	0.064	0.25

Table 2.2 Mix proportion of mortars and concretes for model verification

Designation	Cement (kg/m^3)	Water (kg/m^3)	C. Aggregate (kg/m^3)	Sand (kg/m^3)	Silica Fume (kg/m^3)
M20-MMV	1035	207	-	1035	155
M25-MMV	984	246	-	984	148
M30-MMV	938	281	-	938	141
C20-MMV	717	143	876	717	108
C25-MMV	692	173	846	692	104
C30-MMV	669	201	817	669	100

Table 2.3 Mechanical properties of mortars and aggregate for model verification

Materials	E (GPa)	f_t (MPa)	G_F (N/mm)	ν
M20-MMV	38.5	9.2	0.07	0.24
M25-MMV	36.8	7.8	0.06	0.24
M30-MMV	27.6	5.2	0.06	0.25
Aggregate	98.2	20.8	0.09	0.17

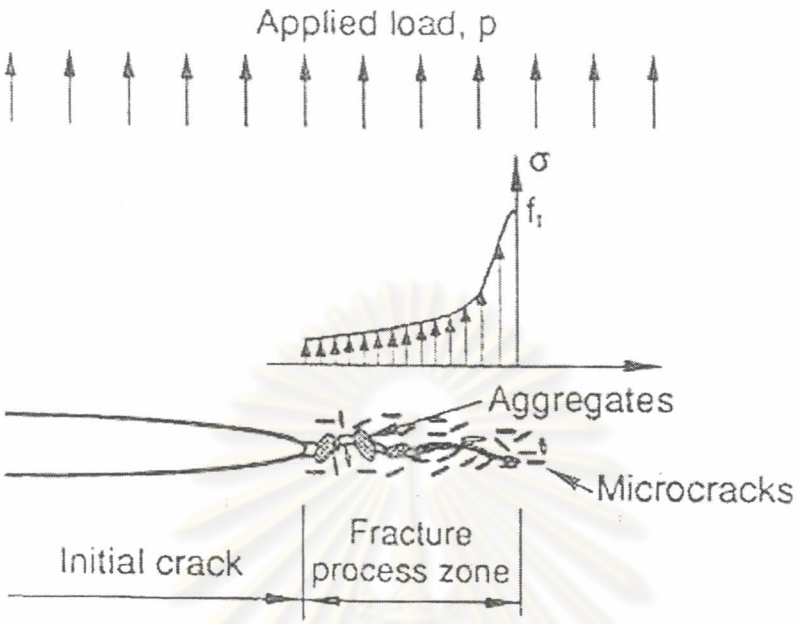

Fig. 2.1 Concrete crack and fracture process zone

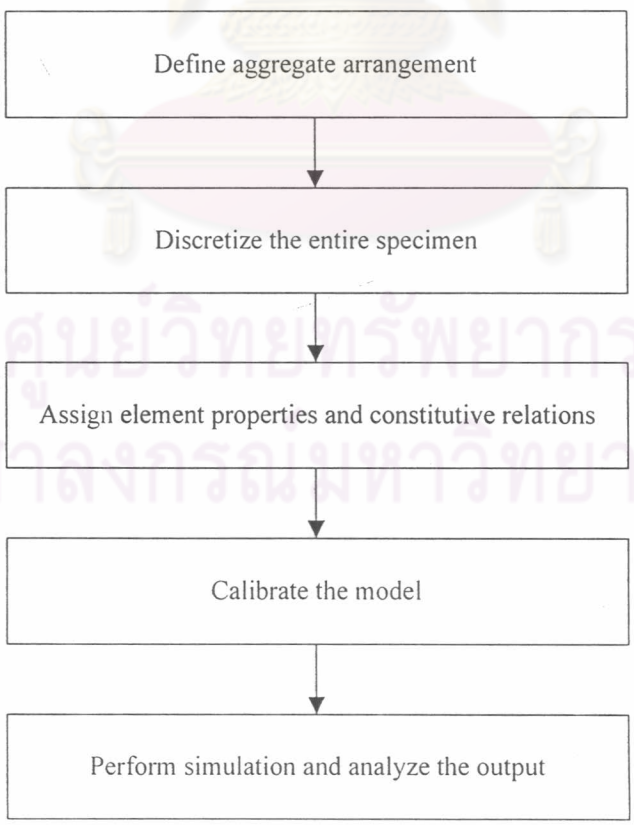

Fig. 2.2 Algorithm for simulation of concrete response

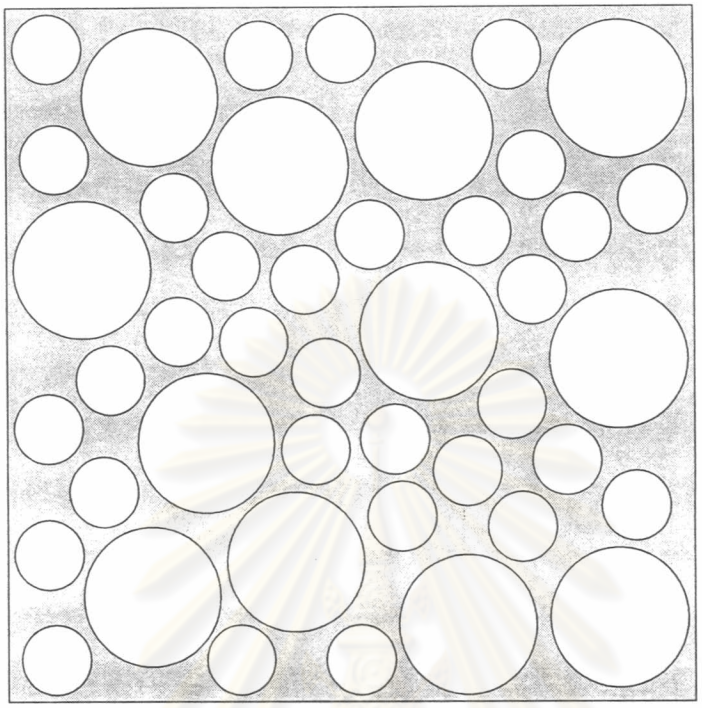

Fig. 2.3 Sample of aggregate arrangement

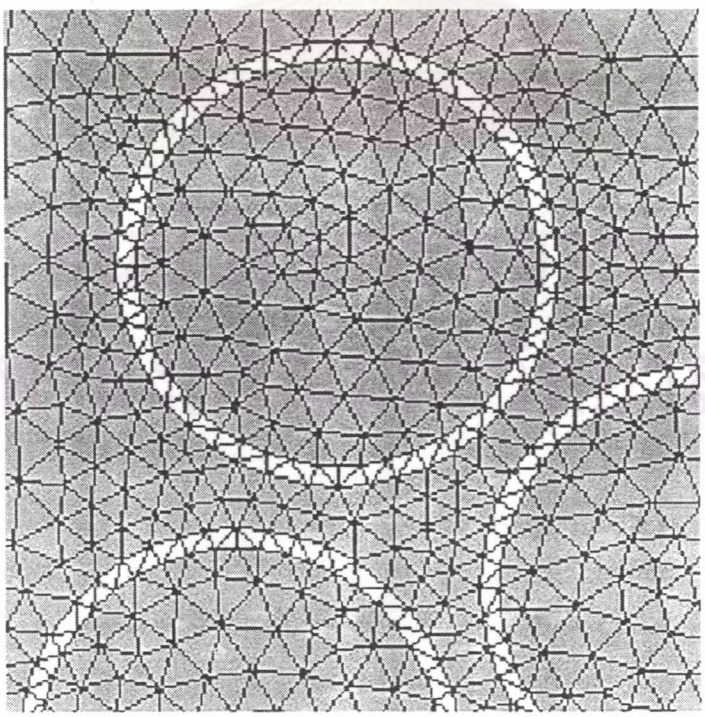

Fig. 2.4 A part of finite element mesh

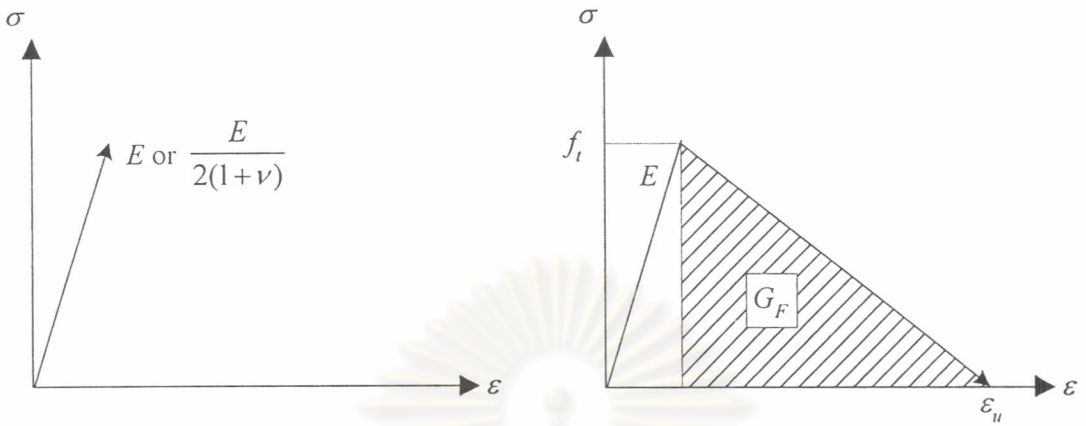

a.) under compressive or shear stress *b.) under tensile stress*

***Fig. 2.5** Element constitutive relations*

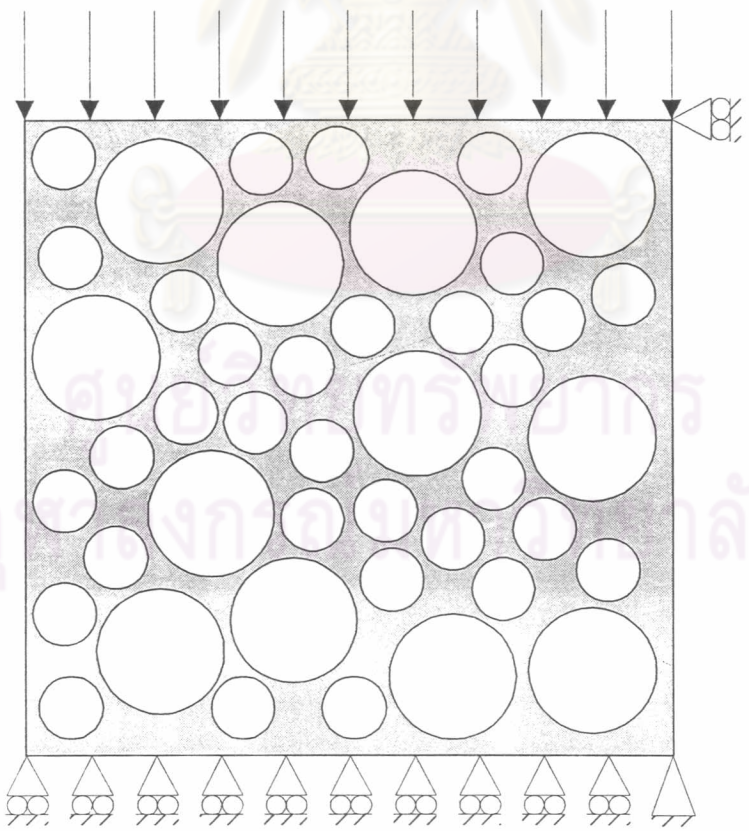

***Fig. 2.6** Boundary conditions for simulation and calibration*

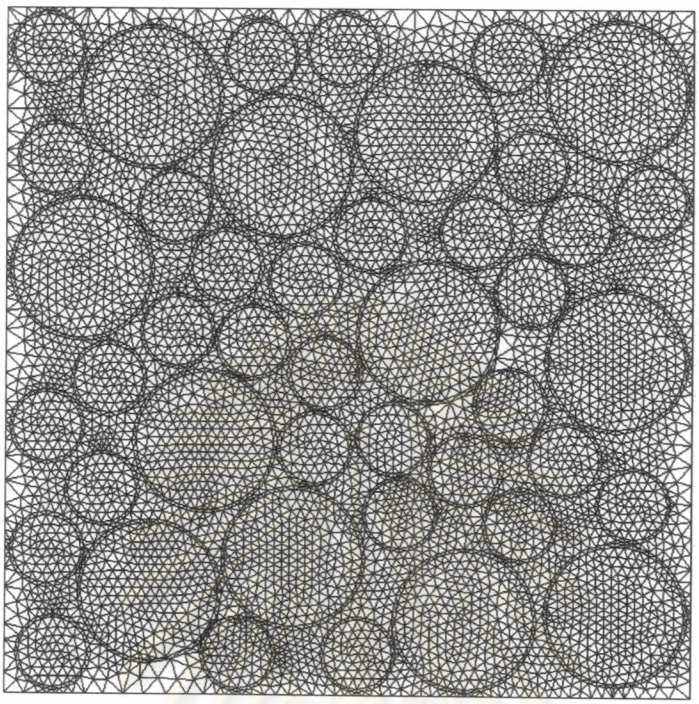

Fig. 2.7 Finite element mesh for simulating compressive response

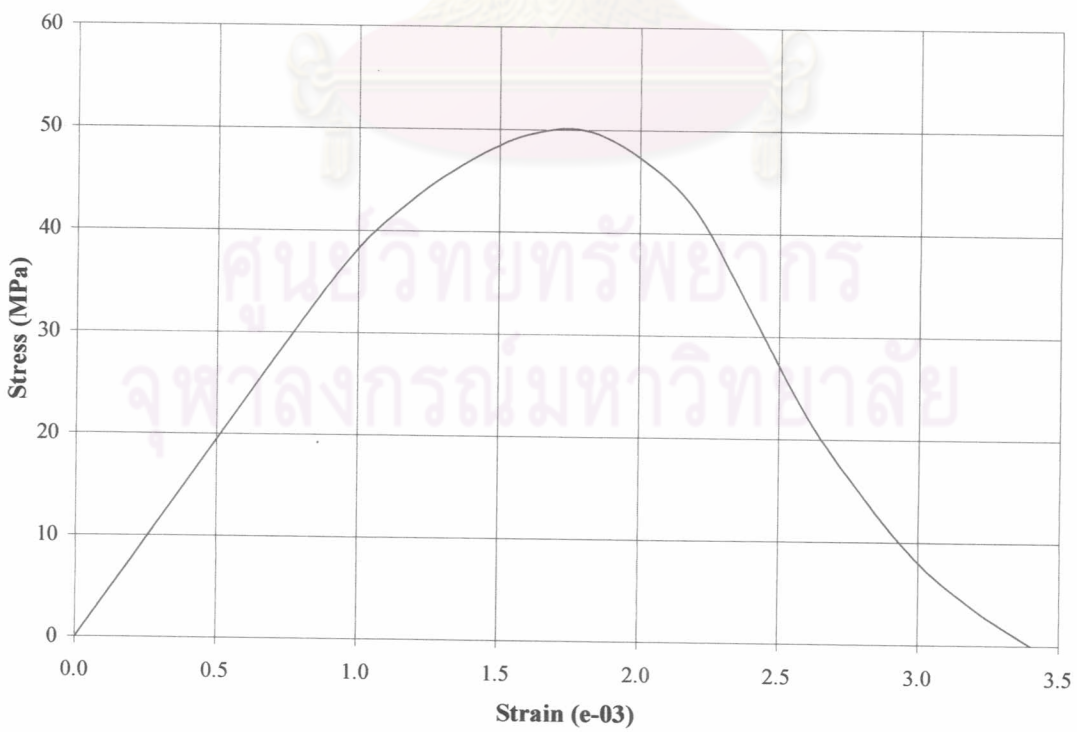

Fig. 2.8 Simulated stress-strain relation of concrete under compressive loading

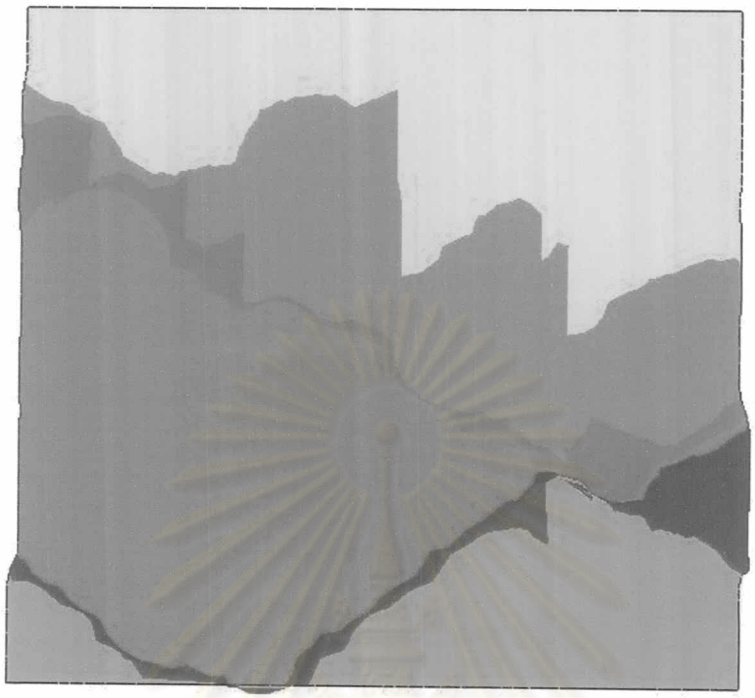

Fig. 2.9 Simulate crack pattern at failure of concrete under compressive loading

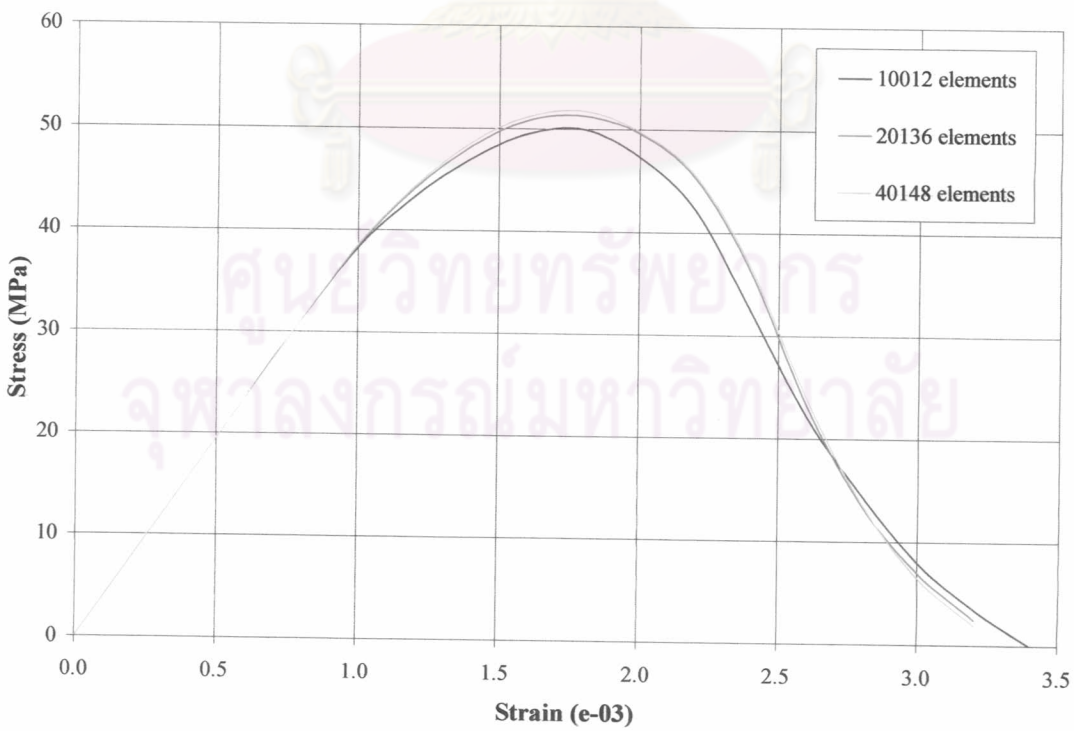

Fig. 2.10 Simulated stress-strain relation of concrete with different number of elements

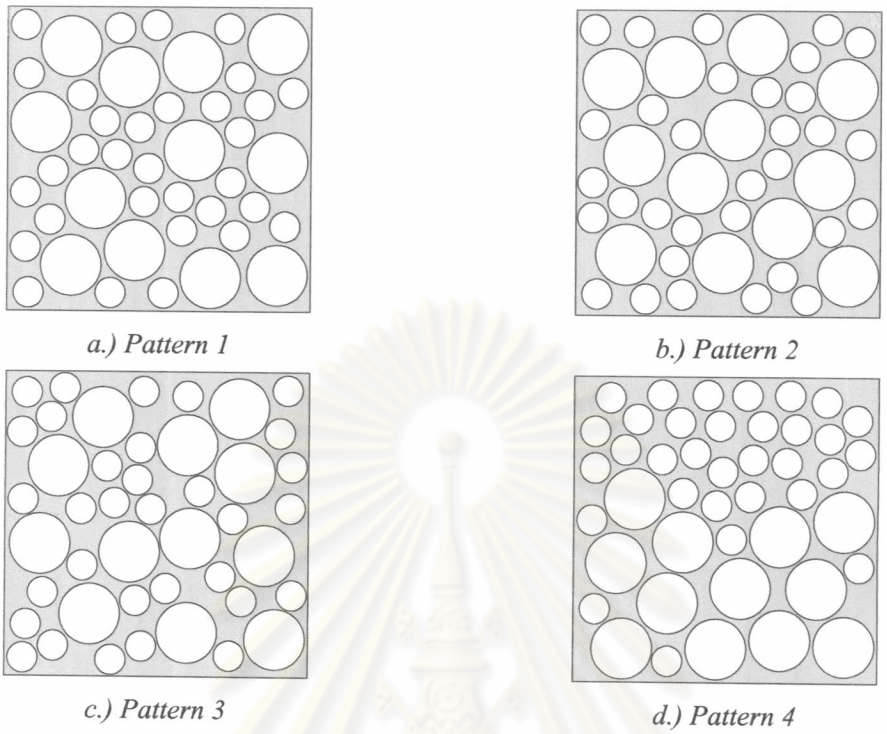

Fig. 2.11 *Patterns of aggregate arrangements*

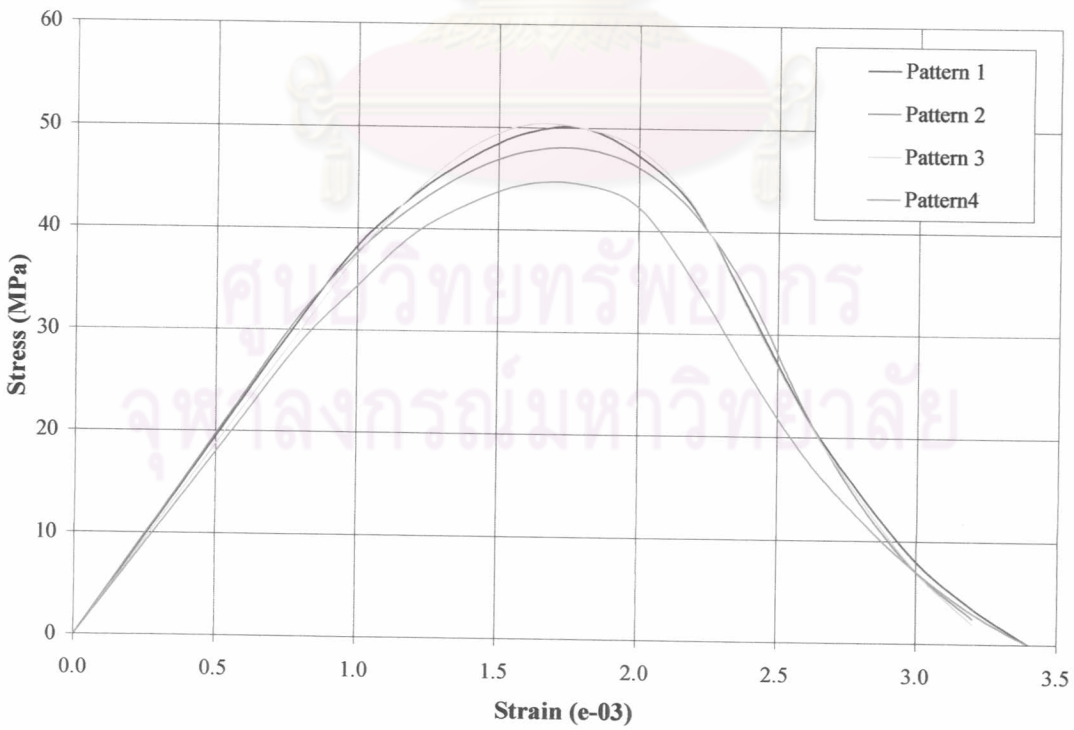

Fig. 2.12 *Simulated stress-strain relation of concrete with different aggregate arrangement*

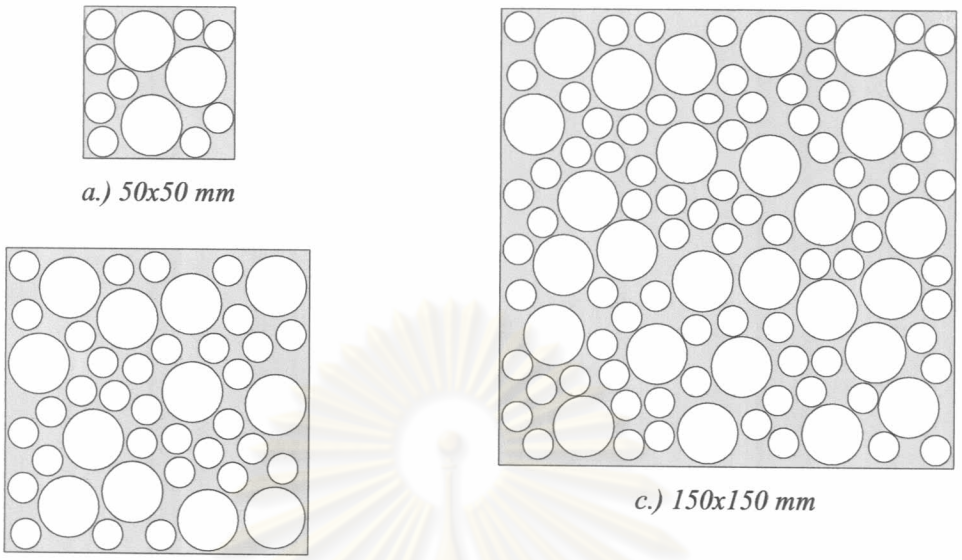

Fig. 2.13 *Concrete specimen with different size*

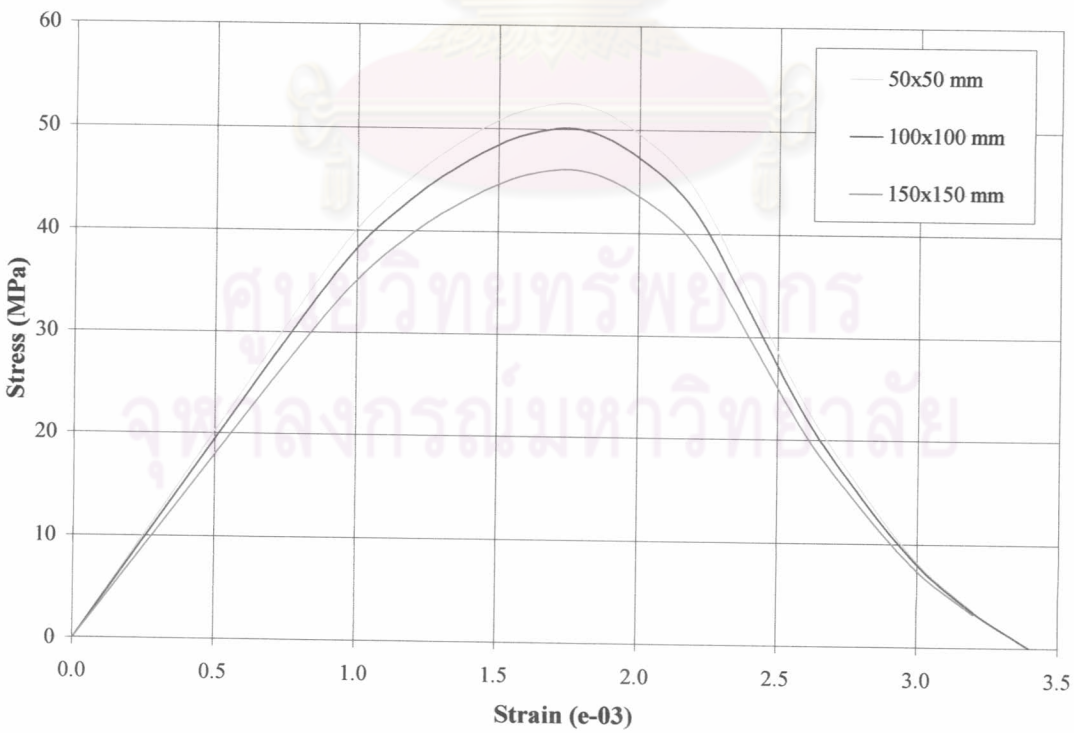

Fig. 2.14 *Simulated stress-strain relation of concrete with different specimen sizes*

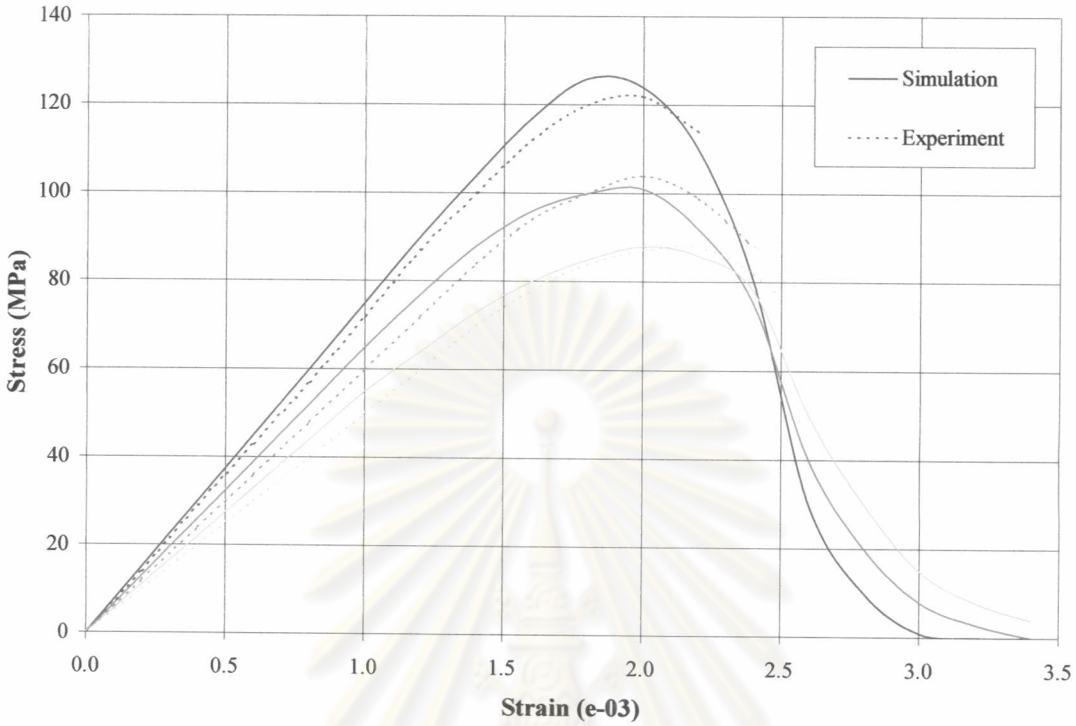

Fig. 2.15 *Comparison of simulated compressive behavior with the experiment*

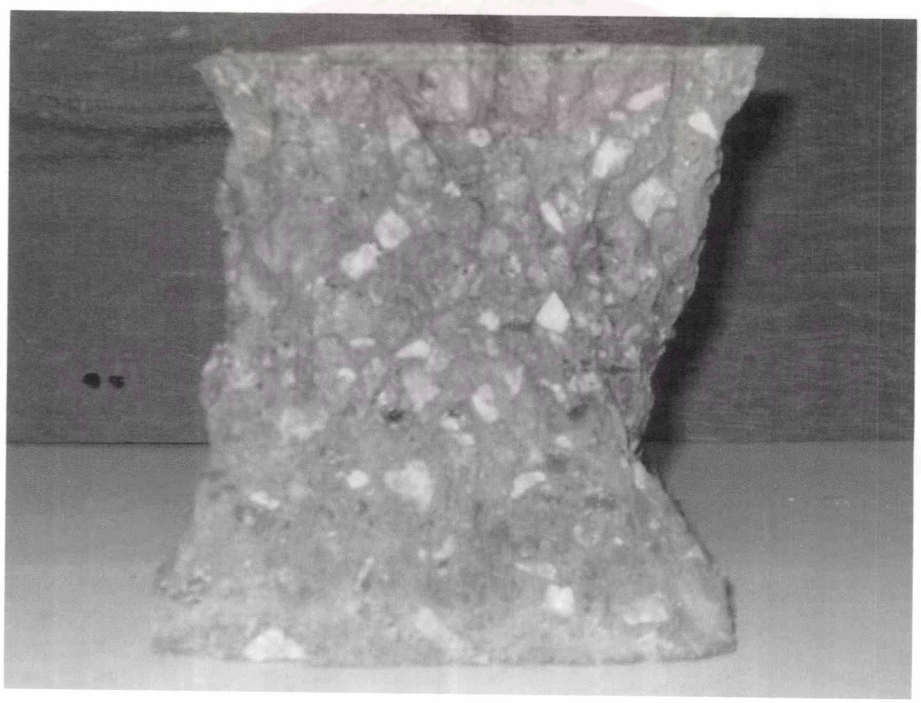

Fig. 2.16 *Failure of concrete specimen under compressive loading*

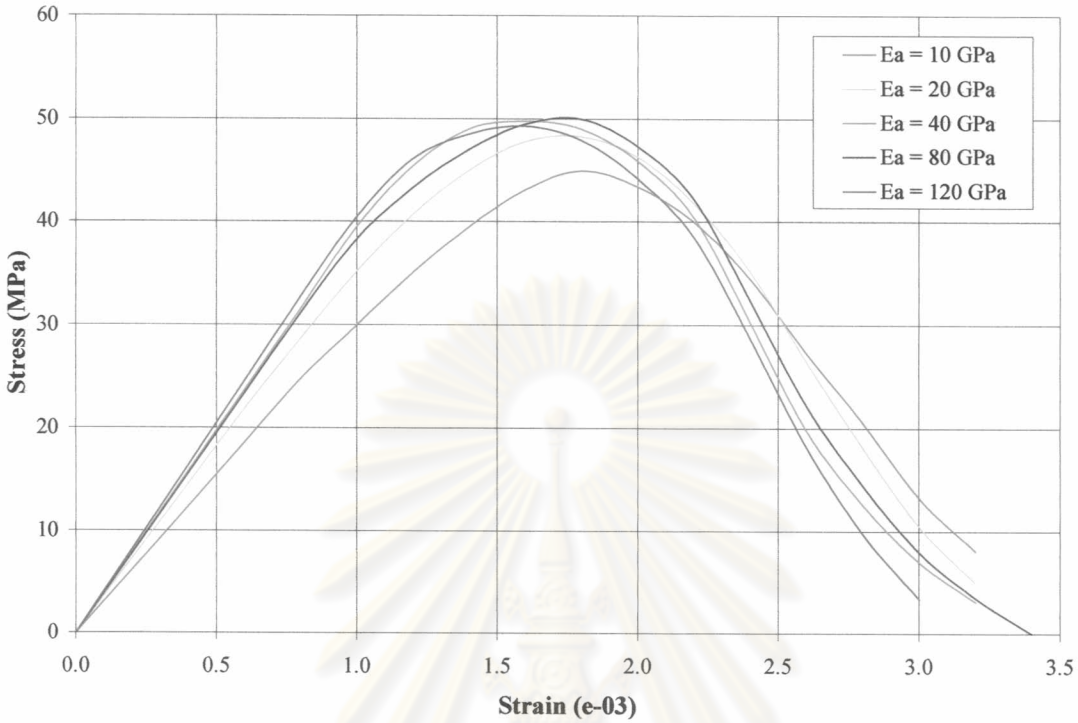

***Fig. 2.17** Stress-strain relationship of concrete with various elastic modulus of aggregate*

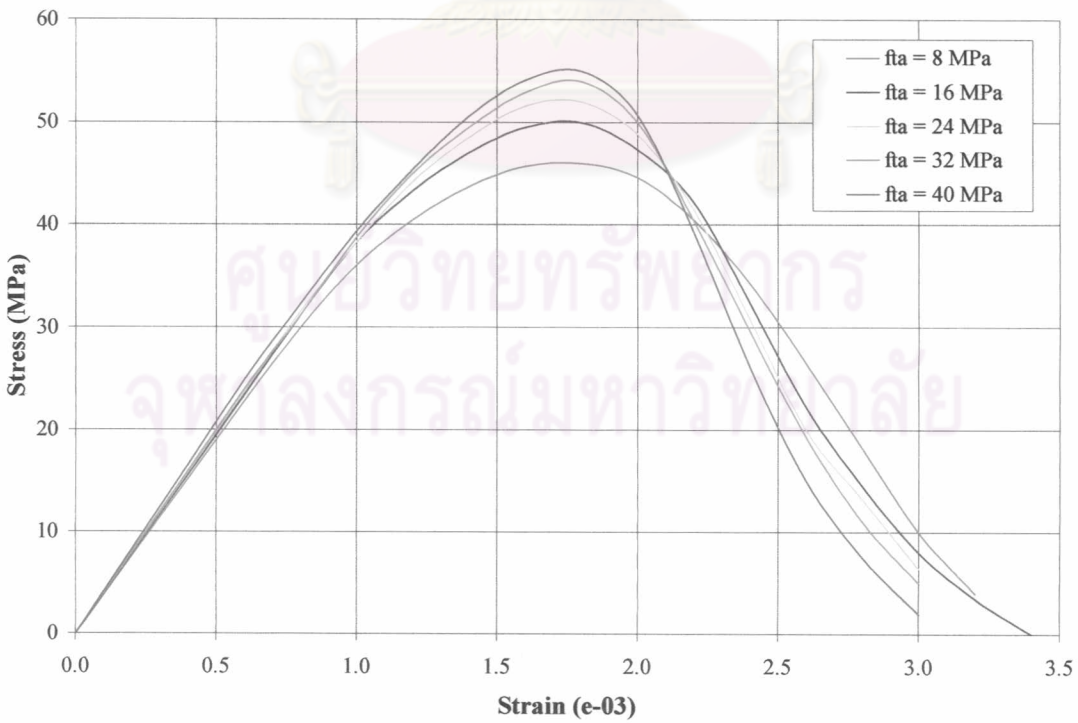

***Fig. 2.18** Stress-strain relationship of concrete with various tensile strength of aggregate*

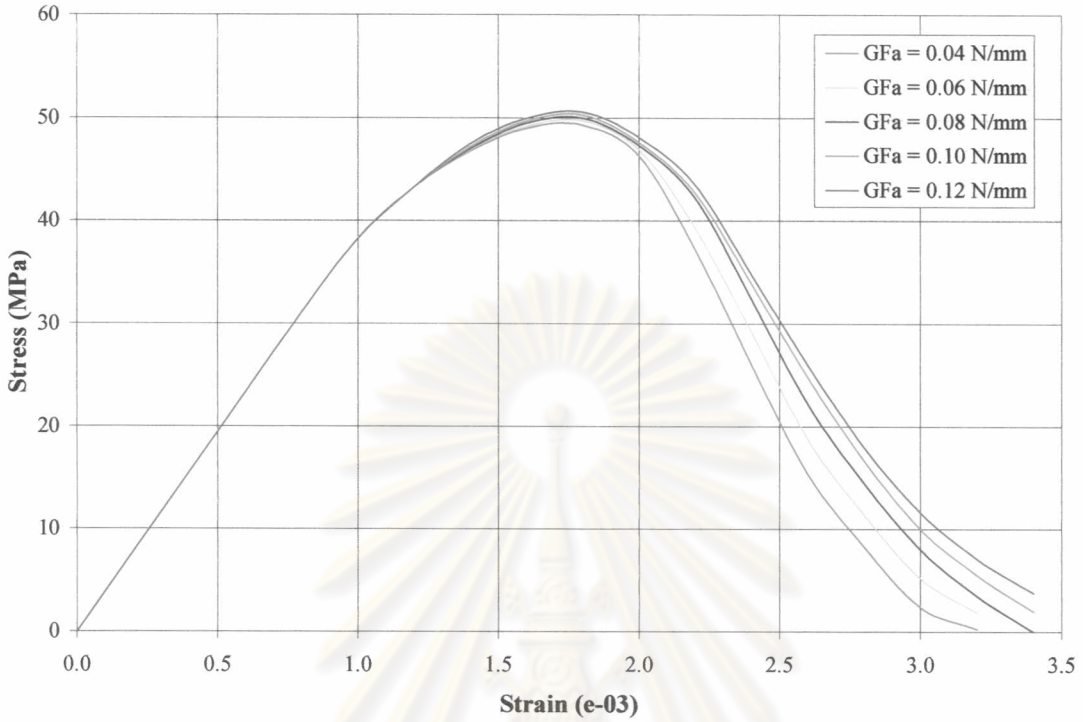

Fig. 2.19 *Stress-strain relationship of concrete with various fracture toughness of aggregate*

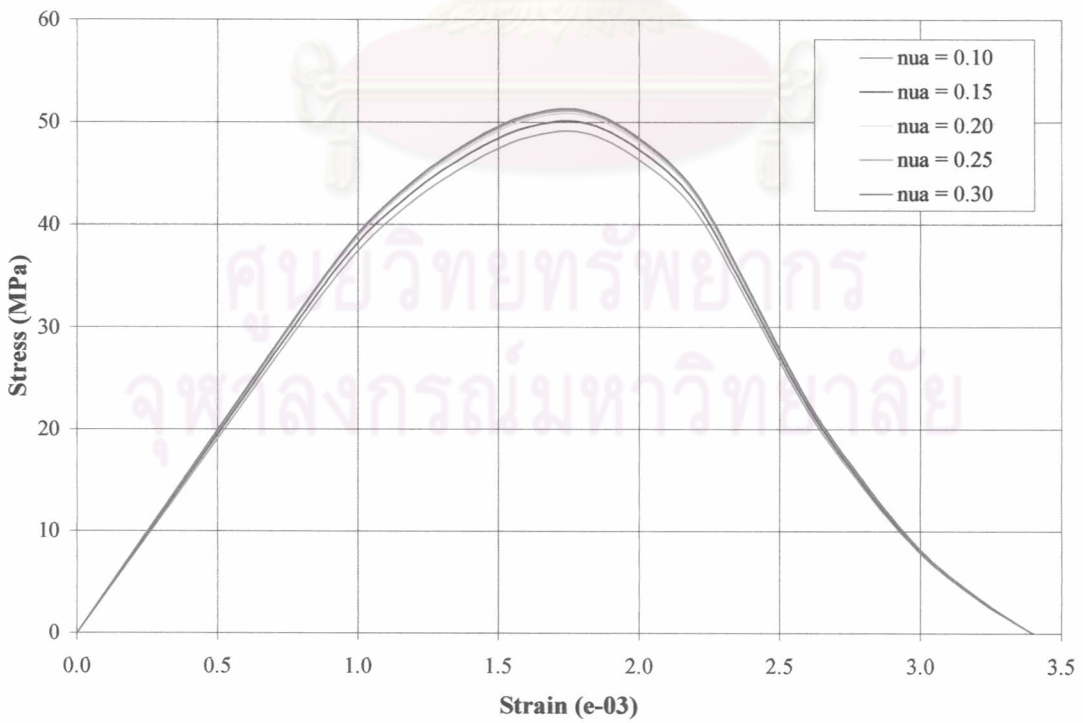

Fig. 2.20 *Stress-strain relationship of concrete with various Poisson's ratio of aggregate*

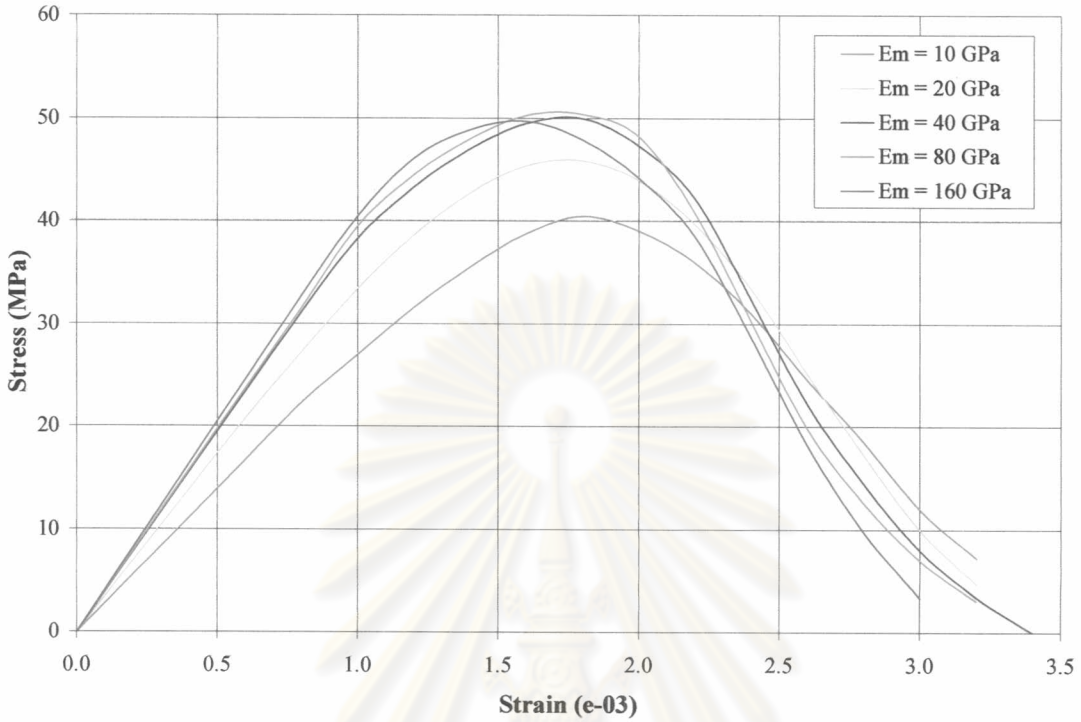

Fig. 2.21 *Stress-strain relationship of concrete with various elastic modulus of matrix*

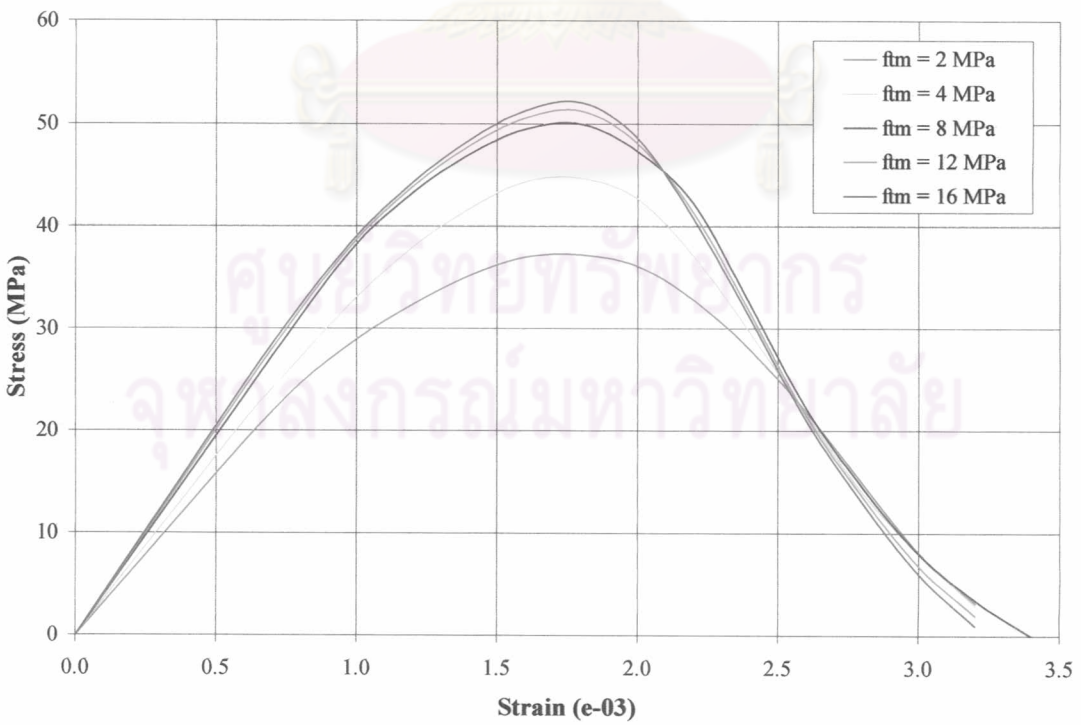

Fig. 2.22 *Stress-strain relationship of concrete with various tensile strength of matrix*

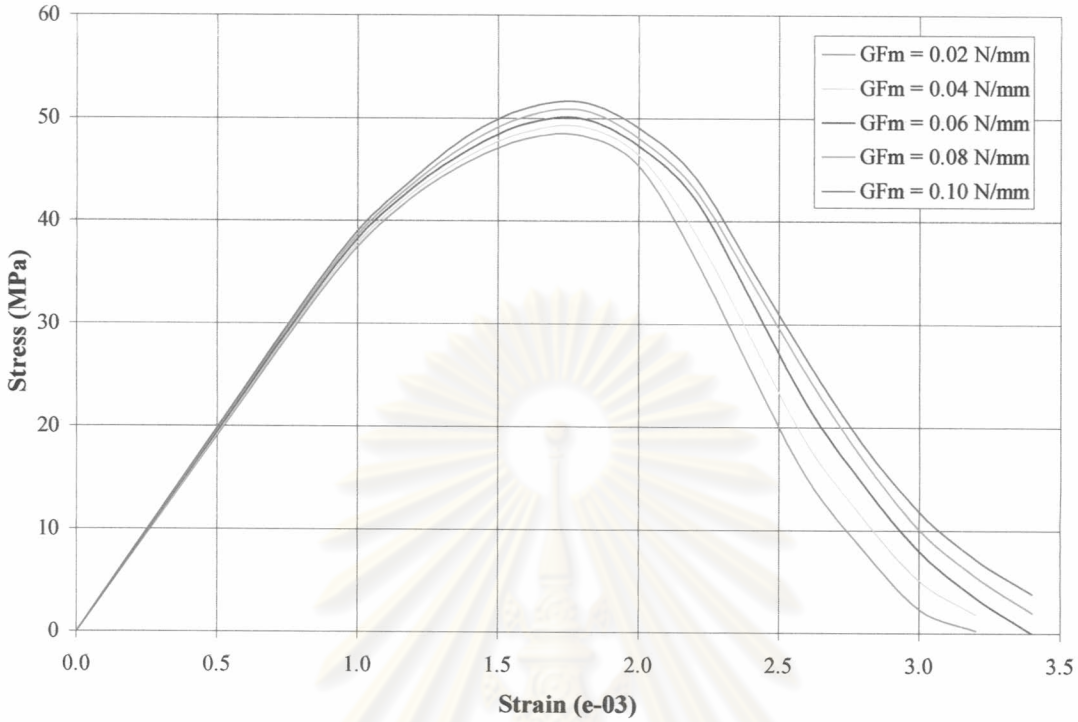

Fig. 2.23 *Stress-strain relationship of concrete with various fracture toughness of matrix*

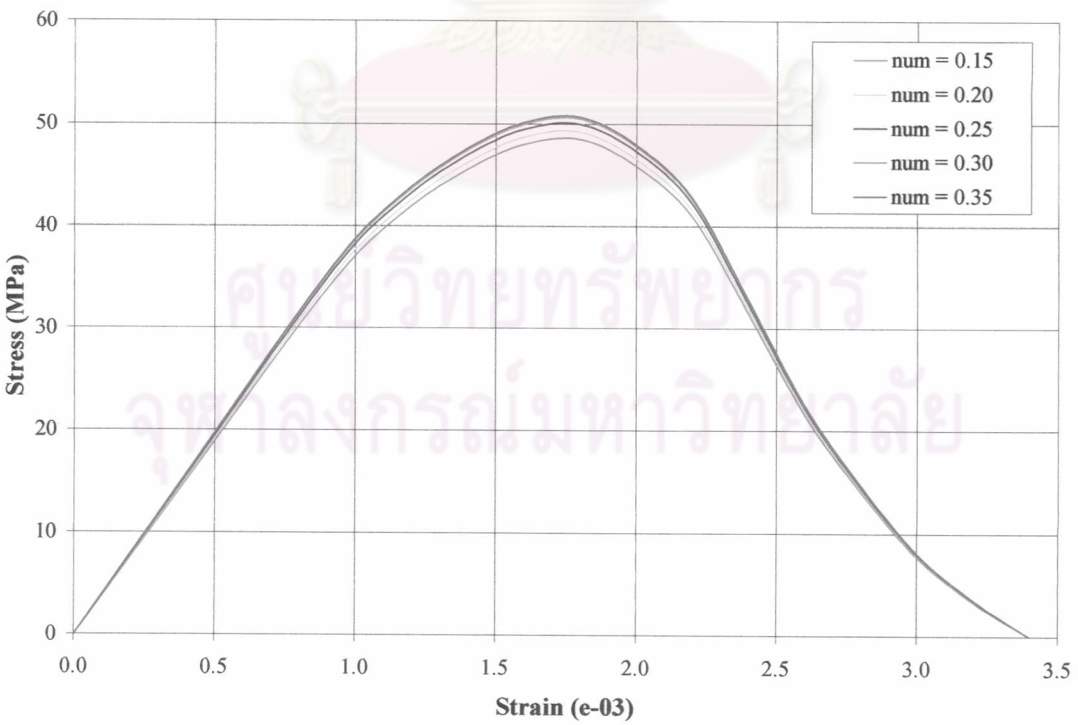

Fig. 2.24 *Stress-strain relationship of concrete with various Poisson's ratio of matrix*

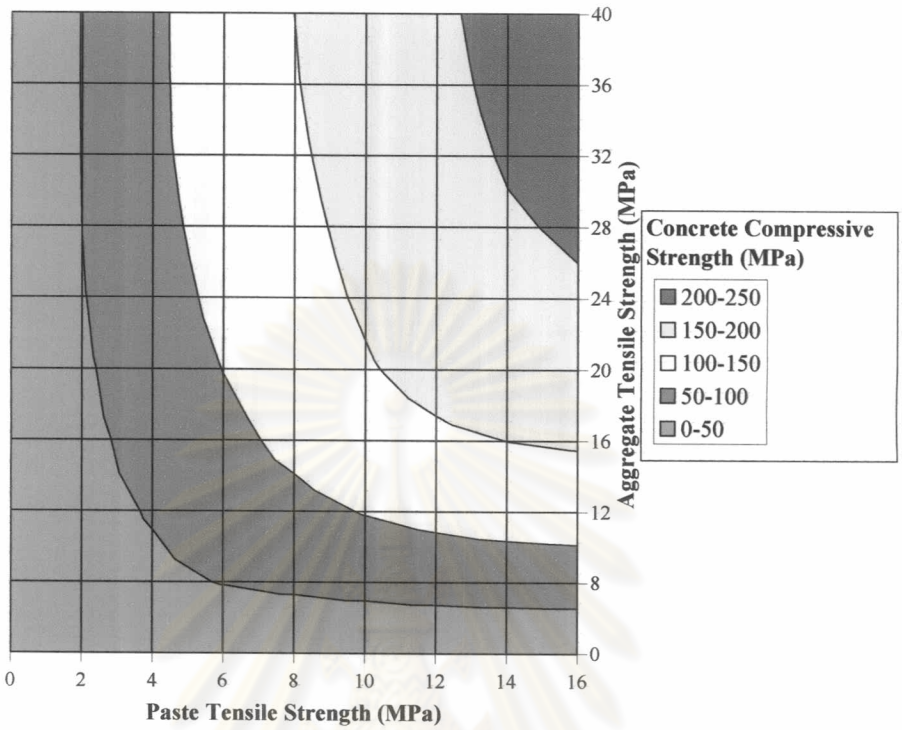

Fig. 2.25 *Contribution of aggregate and matrix tensile strength on concrete compressive strength*